IEEE Access
Multidisciplinary | Rapid Review | Open Access Journal

Received October 6, 2017, accepted October 30, 2017, date of publication November 9, 2017,
date of current version December 22, 2017.

Digital Object Identifier 10.1109/ACCESS.2017.2771799

On Time Compression Overlap-Add Technique in Linear Frequency Modulation Pulse Compression Radar Systems: Design and Performance Evaluation

AHMED YOUSSEF[1], (Student Member, IEEE), PETER F. DRIESSEN[1], (Senior Member, IEEE), FAYEZ GEBALI[1], (Life Senior Member, IEEE), AND BELAID MOA[2]

[1]Department of Electrical and Computer Engineering, University of Victoria, Victoria, BC V8W 2Y2, Canada
[2]Compute Canada/WestGrid/University Systems, University of Victoria, Victoria, BC V8W 2Y2, Canada

Corresponding author: Ahmed Youssef (afyousef@uvic.ca)

ABSTRACT This paper introduces a novel approach to incorporate the time compression overlap-add (TC-OLA) technique used in communication systems into linear frequency modulation pulse compression (LFM-PC) radar systems. This technique significantly boosts the signal-to-noise ratio (SNR) and provides a robust processing gain compared with the traditional radar LFM-PC systems. In addition, TC-OLA provides a better immunity against powerful jamming techniques. At the transmitter side, we divide a digitized LFM chirp signal into a controlled number of overlapping segments. We then speed up each segment by increasing the sampling rate to account for the segment overlap. At the receiver side, we apply OLA to reconstruct the signal with a much higher gain. To simulate and evaluate the performance of the new system, we extend the conventional LFM-PC radar model, which includes matched filter (MF) processor, moving target detector (MTD), and two common constant false alarm rate (CFAR) algorithms, by suitably adding TC and OLA blocks at the transmitter and receiver, respectively. Using the TC-OLA-based LFM radar system, we have control over the SNR level and the spectrum spread while preserving the same Doppler shift and target time delay as the conventional LFM radar system. Furthermore, we transform LFM chirp signal into a novel TC signal that inherits LFM properties while possessing better immunity to jamming. Moreover, the proposed radar model relies on high sample rates only when needed and, therefore, does not require changing MF, MTD, and CFAR as is the case for a wideband LFM radar with the same processing gain. Detailed comparisons between the conventional LFM and the wideband LFM radars against the proposed model are also presented.

INDEX TERMS Communication systems, radar systems, time compression overlap add, linear frequency modulation, signal to noise ratio, jamming, convolution noise jamming, spread spectrum, software defined radar.

I. INTRODUCTION

In the pulse compression technique, radar transmits a relatively long phase or frequency modulated pulse. The received signal is passed through a filter to accumulate the energy to achieve high range resolution capability of short duration [1], [2]. There are various pulse compression waveforms that a radar designer can choose from according to the radar requirements. One of these requirements is to efficiently detect high-speed targets. The LFM waveform is so far the best choice to deal with such a requirement as it has high tolerance to Doppler shift compared to other pulse compression waveforms [3]. Radar designers are also seeking higher processing gains by either enhancing the shape of radar waveforms, or adding modules to the radar receiver without affecting the delay (range), angle and Doppler shift (velocity) of the target. Both of these can be achieved by incorporating Time Compression OverLap Add (TC-OLA) [4], [5] into LFM radar systems.

TC-OLA is a communication scheme that combines two techniques [4], [5]: Time Compression and OverLap-Add.

In Time Compression (TC), the digitally generated signal is divided, at the transmitter, into overlapping segments, and re-sampled using higher rates to produce non-overlapping segments. At the receiver, the signal is reconstructed from the segments using the OverLap-Add (OLA) method.

In the context of TC-OLA-based LFM radar, the designer adds TC and OLA as pre- and post-processing modules at the transmitter and receiver sides of an existing radar to control its processing gain. These modules enhance the LFM waveform at the transmitter side and allow for higher processing gains at the receiver side. Under TC-OLA, we apply TC to the digitized LFM signal and OLA to the received LFM signal to recover the signal with extra gain and undistorted information content (for more details see Section III).

To evaluate the performance of TC-OLA-based LFM radar, a traditional LFM-PC, which contains Matched Filter (MF), MTD, and the two popular CFAR algorithms, Cell Average CFAR (CA-CFAR) and Greatest-Of CFAR (GO-CFAR), is modeled, and then evaluated. After that, TC and OLA are added to the transmitter and receiver respectively, and the modified system is then re-evaluated.

As a further assessment, we subject the two systems to Convolution Noise Jamming (CNJ), one of the modern jamming techniques that is applied to conventional LFM-PC [6]–[8]. Comparing the probability of detection (P_D) versus signal to noise ratio (SNR) under a fixed probability of false alarm (P_{fa}) for both models, we see that the new model has improved immunity against powerful jamming techniques over the conventional model.

Furthermore, the new system has the following features and advantages:

1) No change is required in the radar signal processing blocks: MF, MTD, and CFAR.
2) All the operations are done at lower sampling rate before TC processor and after OLA processor.
3) The radar waveform is a scrambled version of the LFM signal while preserving the vital LFM features and without using any kind of coded sequence. This renders jamming techniques that rely on the nature of LFM signal ineffective.
4) Spectrum spreading and processing gain can be controlled by choosing the appropriate TC and OLA parameters (as discussed in Section III). Moreover, the spectrum spreading introduced is only between TC and OLA processors, and does not propagate to the rest of the corresponding LFM radar components (namely MF, MTD and CFAR).

For the sake of a fair evaluation, we opted to compare the TC-OLA-based LFM against a wideband LFM radar with the same processing gain as our model. The noise and jamming performance, design implications, and software defined radar (SDR) implementation of both show that the two radars have pros and cons. Our proposed model, however, has more features compared to wideband LFM one (for more details see Section VI).

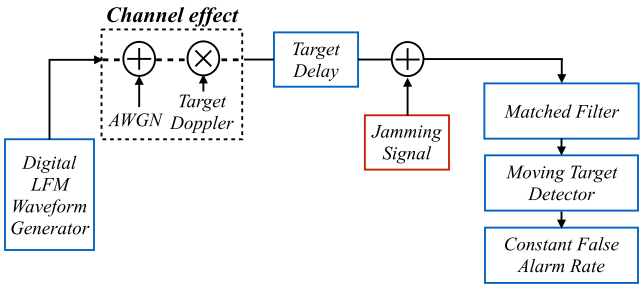

FIGURE 1. Simulated LFM-PC Radar model.

The paper is organized as follows. Section II introduces a brief explanation of LFM-PC radar as well as the parameters of the radar, target, and jammer used. Section III describes TC-OLA theory of operation and the new proposed TC-OLA-based LFM radar model. The evaluation results of the new model are presented and compared against the conventional LFM-PC model. Evaluation of LFM-PC and TC-OLA-based LFM-PC radars under AWGN is discussed in Section IV. As a case study, Section V investigates convolution noise jamming applied to both radar models, and shows the superiority of TC-OLA LFM radar over the conventional LFM-PC radar. The comparison between our proposed model and the corresponding wideband LFM radar is discussed in Section VI. Section VII summaries our paper and discusses our future work. The conventional LFM-PC radar model validation results are deferred to Appendix A.

II. LFM-PC RADAR

A. THEORY OF OPERATION

A block diagram of our simulated LFM-PC radar model is presented in Fig. 1. Once we generate the digital LFM waveform, we subject it to channel effects, including Additive White Gaussian Noise (AWGN), target Doppler shift, and then add target time delay, and jamming signal. The output then goes through each stage of the radar signal processing receiver as discussed next.

The received radar signal is compressed by the MF, a linear filter that gives the maximum SNR at its output. This filter is in the form of a correlator receiver [2], [3]. Its output is feed to the MTD processor where the received Pulse Repetition Intervals (PRIs) are written consecutively into a bulk memory with each PRI occupying a single row. FFT is then performed on each received PRI signal. Because of the Doppler shift, the phasor representation of the data rotates from one sample to the next. The rate at which the phasor rotates is equal to the apparent Doppler frequency. As a result, we obtain a matrix with rows and columns representing the Doppler and range cells, respectively.

The CFAR algorithms are then applied to the resultant matrix for each Doppler cell. The radar detector gives the decision about the presence of the target using W sliding-window cells, which are divided into $W/2$ leading and $W/2$ lagging subwindows, while excluding the two guard cells.

TABLE 1. Simulated parameters of the radar model, the target, and the jamming technique.

Radar Parameters	Symbol	Value	Units
Sampling Frequency	f_s	$2^{26} = 67.1$	MSPS
Pulse Width	δ	100	μs
Pulse Repetition Interval	T_r	500	μs
Carrier Frequency	f_c	3	GHz
Chirp Bandwidth	B	15	MHz
Coherent Pulse Interval	CPI	16	Scaler
Target Parameters	**Symbol**	**Value**	**Units**
Target Range	R_t	185.726	km
Target Doppler	f_d	7	kHz
CFAR Type	CA-CFAR, GO-CFAR		
CFAR Window size	W	8	Range cells
Noise Parameters	**Symbol**	**Value**	**Units**
Additive White Gaussian Noise	AWGN	0	dB
CNJ Parameters	**Symbol**	**Value**	**Units**
Jamming to Signal Ratio	JSR	10, 25, 30, and 35	dB

The adaptive threshold is computed as the mean of the W window cell values, in the case of CA-CFAR, or as the maximum value of the two subwindows, in the case of GO-CFAR. The results obtained are then multiplied by a constant K to give a threshold that is compared with the level of Cell Under Test (CUT) of the target return. The detection occurs when the target-return level crosses that threshold [9]. The K factor has been precomputed to give the desired false alarm rate by injecting noise only to the input of the simulated radar system. Since the number of cells in the sliding window is finite, the background noise is not completely known and loss occurs compared to the ideal detector [3]. Increasing the number of cells decreases the CFAR loss at the expense of increasing the delay of the CFAR processor.

Pulse compression provides the radar receiver with a processing gain equal to the time-bandwidth product of the transmitted pulse [2], [10]. The coherent integration process in modern LFM-PC radar gives an additional processing gain proportional to the length of the Coherent Pulse Interval (CPI) [11]. Using CFAR processing along with pulse compression and coherent integration enhances LFM-PC search radar detection as well as radar immunity against different jamming techniques. More details about the traditional LFM radar model just described are in Appendix A.

B. RADAR, TARGET AND JAMMING PARAMETERS

To choose realistic radar parameters, we reviewed the typical operating radars discussed in [12]–[14] as well as different jamming techniques reported in [6]–[8], [14], and [15]. As we are seeking to compare between conventional LFM-PC radar and TC-OLA-based LFM-PC radar in different situations, we selected the same radar and target parameters as in [14] and opted for AWGN and the smart noise jamming technique CNJ. Table 1 summarizes the radar model, target, noise, and jamming technique parameters. The level of the noise is kept fixed (0 dB) while that of the signal is varied to give a specific SNR.

III. TC-OLA-BASED LFM-PC RADAR

In this section, we present the TC-OLA theory of operations [5] and show how it can be used to implement our new LFM-PC radar model.

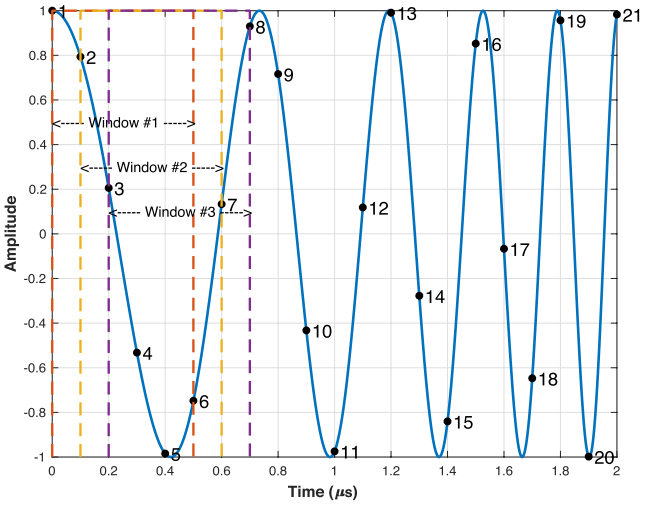

FIGURE 2. Generating overlapping segments from the sampled LFM chirp signal ($M = 5, R = 1$).

A. TC-OLA THEORY OF OPERATION

At the transmitter side, let $x(t)$ be the LFM radar signal and $x[n]$ with length N be its digitized version generated by an ADC at a radar sampling rate f_1. The transmitted radar signal $x_t[n]$ is generated by concatenating the sequence of segments $(S_j), j \in [0, \frac{N-M}{R}]$, where M is the segment length, R is the hop size, each S_j is a vector of length M defined as follows:

$$S_j = \Big[x(jR), x(1+jR), \ldots, x(M-1+jR)\Big]. \tag{1}$$

To express $x_t[n]$, a windowing function is introduced to select the proper segment via a shift. Since each segment overlaps with the next by $M-R$ samples, $n-i(M-R)$ gives the index of the transmitted value in the segment i. Therefore, $x_t[n]$ can be written as:

$$x_t[n] = \sum_{i=0}^{N-M+1} w(n-iM)x(n-i(M-R)), \tag{2}$$

where $w(n)$ is a windowing function that can be of any digital window function type [16]. The support of the windowing function, however, has to be $[0, M-1]$. To cover only the finite length of the signal, the overlapping process should end at $N-M+1$. After the overlapping segment process, we obtain a redundant signal that spans $\frac{M}{R}$ of the time interval of the original signal. To preserve the time (length) of the original signal $x(t)$, $x_t[n]$ is converted to continuous-time signal $x_t(t)$ by DAC at a high sampling rate $f_2 = \frac{M}{R} f_1$. This process is called *time compression* and is illustrated in Fig. 2 and Fig. 3.

In Fig. 2, we show the first 2 μs of the LFM signal (based on the parameters shown in in Table 1 and Table 2), as well as the overlapping segments. The LFM signal is sampled at each 0.1 μs. The overlapping segments are produced by using a rectangular window function of width 0.4 μs. The windowing function slides along the LFM signal according to the hop size $R = 1$ (equivalent to 0.1 μs). Speeding up the rate of the

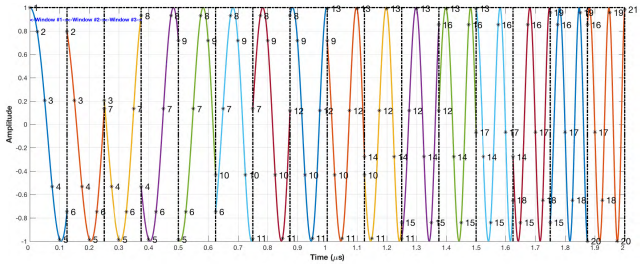

FIGURE 3. The new chirp signal after increasing sampling rate from f_s to $f_2 = \frac{M}{R} f_s$ ($M = 5, R = 1$) to ensure non-overlapped segments.

TABLE 2. TC-OLA Parameters.

Signal Parameters	Symbol	Value	Units
Sampling frequency # 1	f_1	$2^{26} = 67.1$	MHz
Segment length	M	5	Samples
Hop size	R	1	Samples
Sampling frequency # 2	f_2	$5 * 2^{26} = 335.5$	MHz

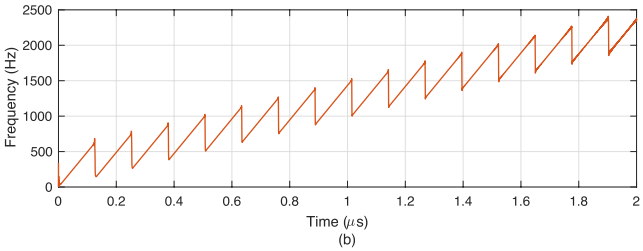

FIGURE 4. Instantaneous frequency for non-overlapped segments after applying Hanning window.

signal to $f_2 = \frac{M}{R} f_s$ makes the segments no longer overlap and leads to a new chirp signal, TC chirp signal, shown in Fig. 3.

The instantaneous frequency of the new produced chirp signal is shown in Fig. 4. The spectrogram of the time-frequency complex baseband LFM chirp signal and the TC chirp signal are shown in Fig. 5 and Fig. 6, respectively. Because of the increase of the sampling rate from f_1 to f_2, the spectrum of TC LFM signal is spread over a large bandwidth that extends up to $\frac{M}{R} f_1$ as shown in Fig. 6.

At the receiver side, the received signal $x_r(t)$ is re-sampled via ADC at the sampling rate f_2 to obtain a discrete-time signal $x_r(n)$. To recover the original LFM chirp signal from the TC chirp, we need to deploy the overlap-add processor, which first partitions $x_r(n)$ into consecutive segments of length M. Each segment is then shifted to the right by R with respect to its preceding segment and added to produce the final signal x_f. The shifting is carried out using the windowing function w to produce overlapping segments similar to the ones at the transmitter side. For a segment i and given that now the segments overlap over $M - R$, $n + i(M - R)$ gives the index of the value of x corresponding to the index n of the final reconstructed signal x_f. Therefore, x_f can be expressed as:

$$x_f(n) = \sum_{i=0}^{N-M+1} w(n - iR) x_r(n + i(M - R)). \qquad (3)$$

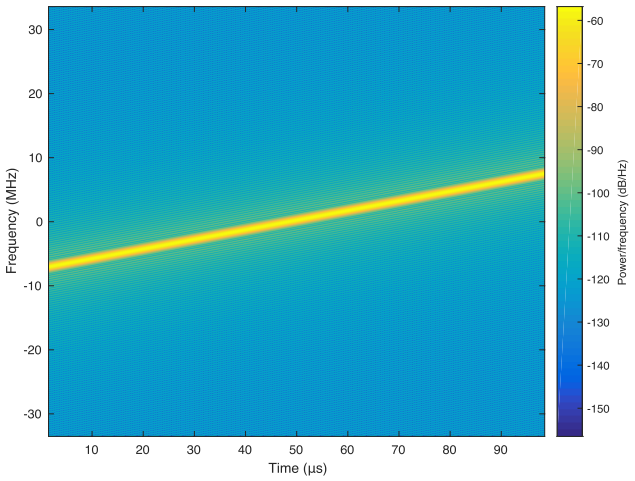

FIGURE 5. Spectrogram of LFM chirp signal.

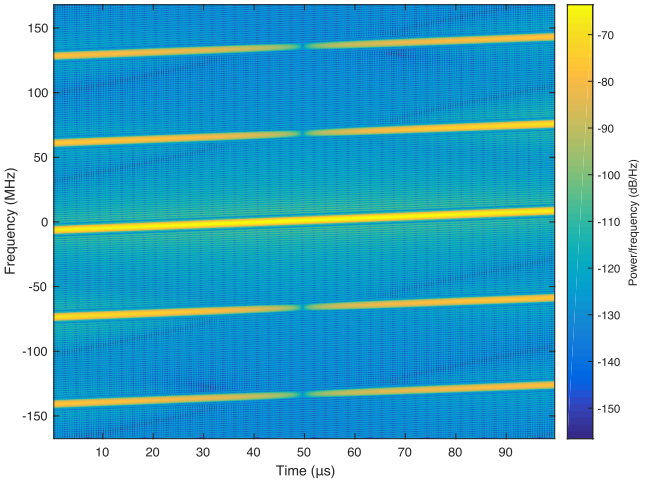

FIGURE 6. Spectrogram of the TC LFM chirp signal. The spectrum is spread over $\frac{M}{R} f_1$.

By taking w to be a rectangular window function, we see that the gain of the received signal is increased by a factor of $\frac{M}{R}$ [4]. All processors coming after OLA carry out their operations at a lower sampling rate, f_1. Recalling the parameters mentioned in Table 2, $M = 5$ and $R = 1$, the processing gain of OLA is approximately equal to 7 dB over the gain of LFM chirp signal while preserving the shape of LFM chirp signal as in Fig. 5.

With this short description of TC-OLA, we are ready to combine TC-OLA and LFM-PC, and produce a new radar model (TC-OLA-based LFM-PC radar) as described next.

B. TC-OLA-BASED LFM-PC RADAR

A block diagram of the new proposed TC-OLA-based LFM-PC radar is shown in Fig. 7. As we are seeking a comparison between the performance of the LFM-PC and the TC-OLA LFM models, we subject the latter to the same channel effects (namely AWGN and target Doppler), target

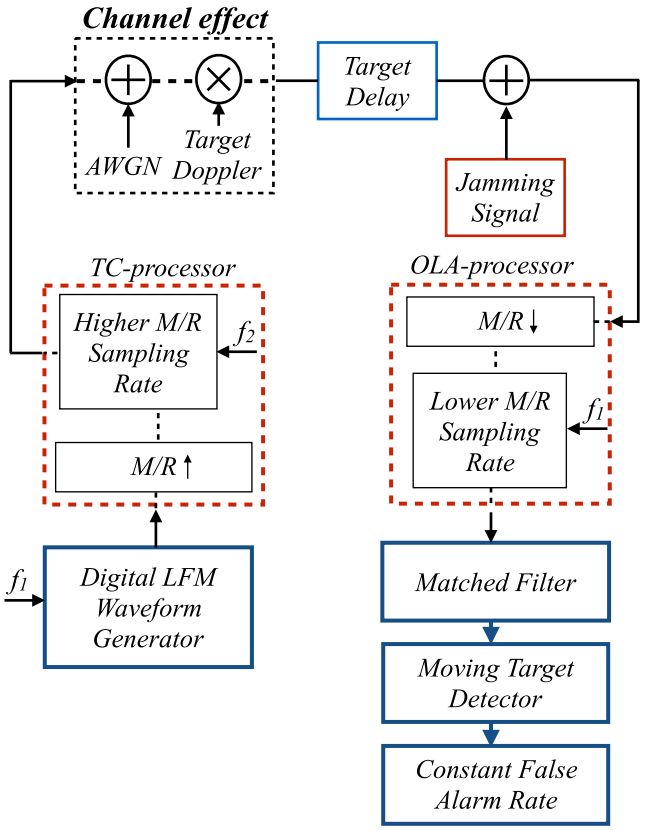

FIGURE 7. TC-OLA-based LFM-PC Radar Block.

time delay, and jamming signal as the former. After that, the OLA processor transforms the received high-rate signal by overlapping and adding the signal according to the parameters M and R, and then decreasing the sampling rate from f_2 to f_1. At this stage, we have the same version of the traditional LFM chirp signal but with an extra gain of $\frac{M}{R}$.

The advantage of combining TC-OLA with LFM-PC radar is that we are able to increase SNR as well as spread the spectrum of the signal while preserving the same received data information (i.e. same Doppler shift and target time delay) as the traditional LFM signal. In TC-OLA-based LFM-PC, target time delay is the same as the traditional LFM-PC radar since time compression is used to avoid any time expansion at the transmitter side. At the receiver side and after OLA, the signal is back to its normal low rate nature and, therefore, regains its original time scale. To ensure that the Doppler shift does not affect the repeated samples, TC-OLA parameters (M, R) and Doppler shift should satisfy the following condition (see Appendix VII-B for the details):

$$M \ll \frac{f_1}{f_c}\frac{c}{2v_r}, \tag{4}$$

where f_1 is sampling frequency, f_c is the radar carrier frequency, c is the speed of light, and v_r is the target relative velocity. In practice, this condition is easily satisfied. In fact, for the fastest aircraft in the world, North American X-15 [17], the velocity is equal to 7200km/h. Therefore,

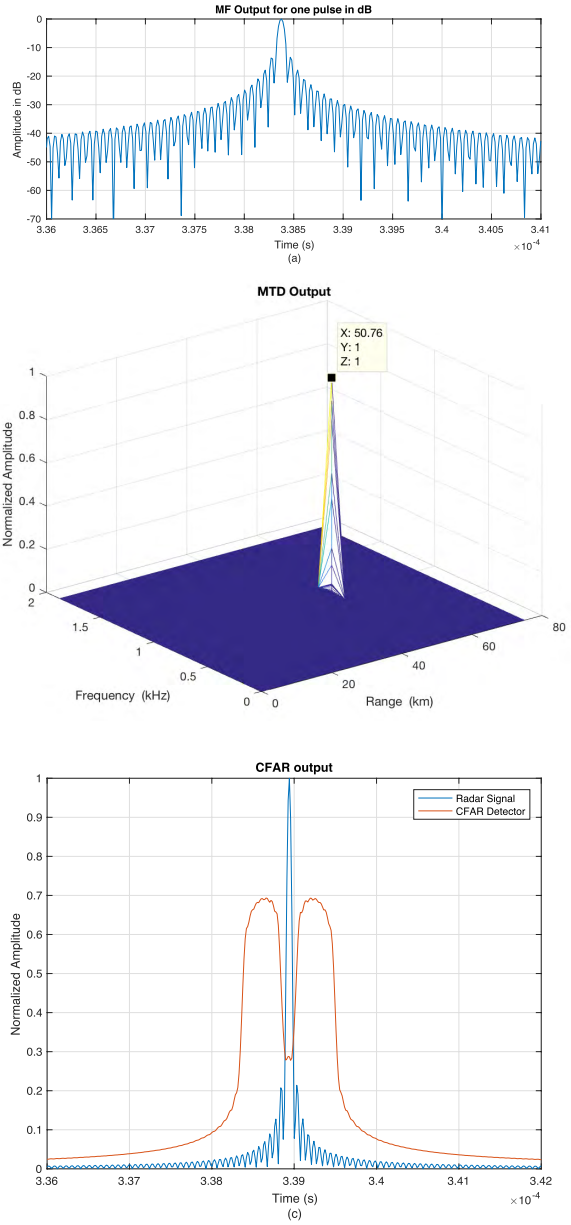

FIGURE 8. The response of the proposed TC-OLA-based LFM-PC radar model. (a) The output of the MF, (b) The Output of MTD, and (c) The Output of the CFAR detector.

to preserve the Doppler signal, the length $M \ll 1675$ samples, which is satisfied for values of M such as 20.

Fig. 8 shows the output of the MF, MTD, and CFAR, respectively. There is no difference between the normalized outputs of the new model, and that of the LFM-PC radar model described in Appendix A from Fig. 21 to Fig. 25.

IV. EVALUATION OF LFM-PC AND TC-OLA-BASED LFM-PC RADARS UNDER AWGN

The radar performance evaluation is done through the well-known curve that combines SNR, P_D (probability of detection), and P_{fa} (false alarm rate), we call it "P_D vs SNR curve." This curve helps in analyzing one variable versus another

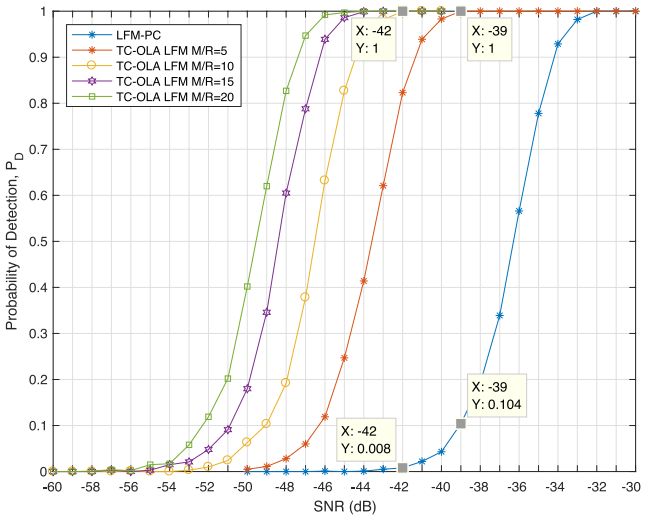

FIGURE 9. P_D vs *SNR* curve for traditional LFM-PC and new TC-OLA-based LFM-PC models at $P_{fa} = 10^{-6}$ under AWGN effect. For new model $\frac{M}{R} = 5, 10, 15, 20$.

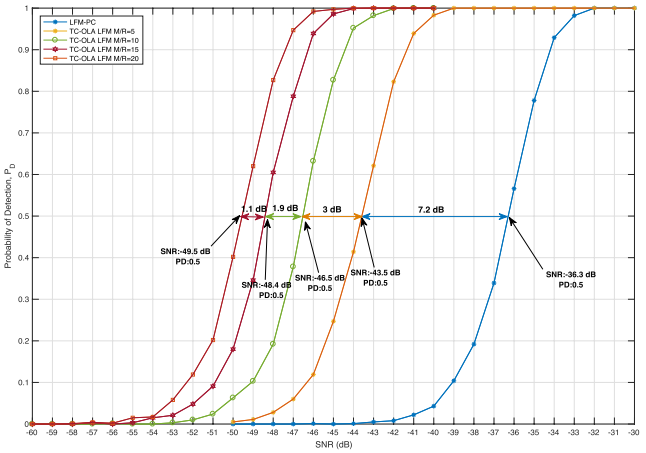

FIGURE 10. P_D vs *SNR* curve for traditional LFM-PC and new TC-OLA-based LFM-PC models at $P_D = 0.5$ and $P_{fa} = 10^{-6}$ under AWGN effect. For new model $\frac{M}{R} = 5, 10, 15, 20$.

while keeping the third fixed [9]. In our case, we analyze SNR with respect to P_D for the given P_{fa} value of 10^{-6}. As mentioned in Appendix A, this value is a common value in radar design and is enforced by injecting AWGN only to the radar model and computing the K factor that ensures $P_{fa} = 10^{-6}$.

Based on the Neyman-Pearson criterion, the radar probability of detection P_D is given by [2]:

$$P_D \approx 0.5 \times erfc\left(\sqrt{-\ln(P_{fa})} - \sqrt{SNR + 0.5}\right), \quad (5)$$

where $erfc(.)$ is the complementary error function expressed as:

$$erfc\,(x) = 1 - \frac{2}{\sqrt{\pi}} \int_0^x e^{-z^2} dz. \quad (6)$$

The simulated as well as theoretical P_D vs *SNR* curve for the conventional LFM-PC radar model with CA-CFAR and GO-CFAR detectors is shown in Fig. 26 in Appendix A.

Since there is no significant difference between the outputs of the two CFAR detectors as shown in Appendix A, we carry out the rest of the analysis and the evaluation based on CA-CFAR only.

Fig. 9 shows the comparison between the traditional LFM-PC model and the new proposed TC-OLA-based LFM-PC model for different $\frac{M}{R}$ values. At SNR $= -39$ dB and $\frac{M}{R} = 5$, for example, the P_D of the new model reaches 100% while the traditional model has only $P_D = 10\%$. Also, at SNR $= -42$ dB and $\frac{M}{R} = 10$, the P_D of the new model reaches 100% while the traditional model has approximately 0% detection. As $\frac{M}{R}$ increases, the P_D increases accordingly and shows the superior performance of TC-OLA LFM over the LFM-PC model: the SNR can be controlled by modifying the TC-OLA parameters M and R. If we happen to fix P_D to, say 0.5, then we can easily see that we require extra $(10 \log_{10} \frac{M}{R})$ dB SNR in the case of LFM-PC to achieve $P_D = 0.5$ (for $\frac{M}{R} = 10$, we gain extra 10 dB over the traditional LFM-PC) as shown in Fig. 10.

It worth emphasizing that, in addition to the gain increase, we also spread the spectrum over a larger band as discussed in the previous section.

Increasing $\frac{M}{R}$ implies increasing the sampling rate of TC and OLA processors. This could be a limitation in our radar design, but with the current high sampling rate devices, such a limitation is surmountable. For example, Xilinx has recently introduced high-speed RF designs with 4 GSPS ADCs and 6.4 GSPS DACs [18], [19]. This new technology supports our approach and allows for flexible TC-OLA designs to achieve higher SNR and spread the spectrum of the signal. One significant advantage is that the MF, MTD and CFAR processing is done at the low sampling rate f_1 thus maintaining the same processing power requirements with and without TC-OLA technique.

V. EVALUATION OF LFM-PC AND TC-OLA-BASED LFM-PC RADAR UNDER CNJ

With the significant improvement in detection of the TC-OLA-based LFM-PC radar over the conventional one, it is worth assessing it under a powerful jamming technique. Convolution jamming is considered one of the smart noise jamming techniques [6], [7] that were specifically proposed for jamming LFM radars [20]. The idea is that instead of transmitting high-power jamming signals, the jammer receives the radar signal and convolves it with random signals. By doing so, less power is required to effectively jam the signal compared to other jamming techniques such as blanket jamming [21].

Let us assume that the intercepted LFM signal or TC-OLA-based LFM signal at the self screening jammer (SSJ), a unit carries jamming equipment for its own protection, located at a distance $R_j = R_t$ from the radar is given by [6]:

$$S_{rj}(t) = S(t) \otimes \delta(t - t_j), \quad (7)$$

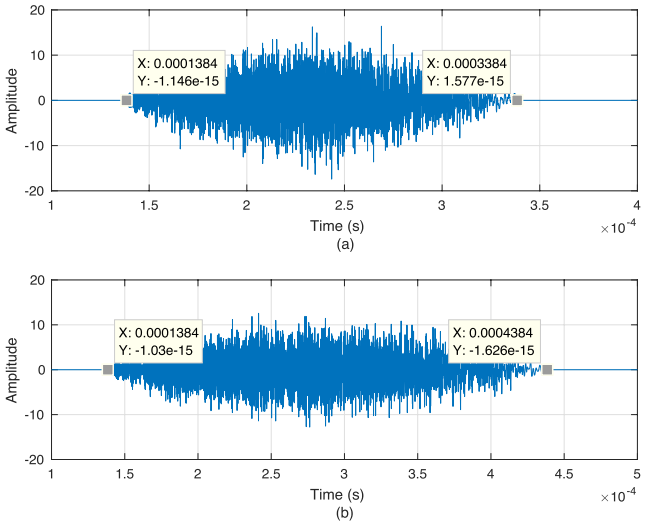

FIGURE 11. Jamming pulse only. (a) Jamming pulse before MF; It has twice time duration with respect to radar pulse duration. (b) Jamming pulse after MF; It has three time duration of radar pulse width.

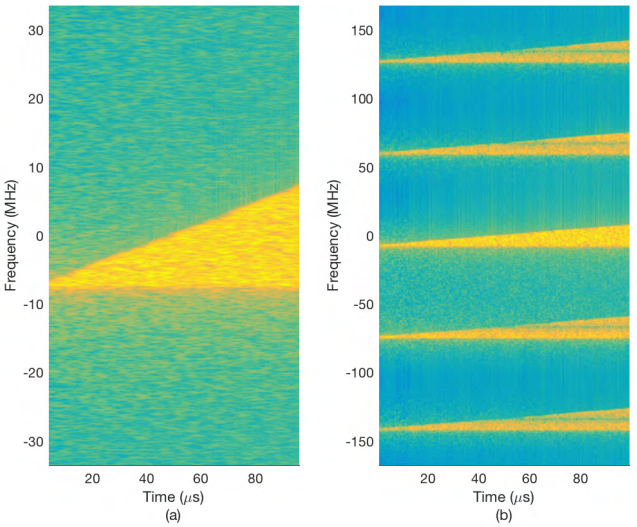

FIGURE 12. (a) Spectrogram represents CNJ signal based on LFM signal. (b) Spectrogram represents CNJ signal based on TC LFM signal.

where $S(t) = ae^{j\pi\mu t^2}$, μ is the chirp rate, in the case of conventional LFM-PC radar or $S(t) = x_t(t)$, the continuous-time signal (see Eq. 2), in the case of TC-OLA-based LFM-PC radar, t_j is the time delay of the signal expressed as R_j/c. The convolution noise jamming signal is:

$$J(t) = S_{rj}(t) \otimes n(t) \otimes \delta(t - t_o), \tag{8}$$

where $J(t)$ is the pulsed jamming signal, $n(t)$ is the white Gaussian noise, t_o is the time delay of the transmitted jamming signal. The received jamming signal by the LFM-PC radar or TC-OLA-based LFM-PC radar is therefore:

$$\begin{aligned} x_j(t) &= J(t) \otimes \delta(t - t_j) \\ &= S(t) \otimes \delta(t - t_d) \otimes n(t), \end{aligned} \tag{9}$$

where $t_d = 2t_j + t_0$. From Eq. 8, we can deduce that the convolution noise jamming signal has twice the pulse width of the radar signal. At the radar receiver, after compression, it would be three times the pulse width of the radar signal. Fig. 11 illustrates that our simulation is consistent with this observation.

The effect of CNJ on the LFM signal and TC-OLA-based LFM signal is shown in Fig. 12. The CNJ managed to spread all the power of the noise over the full bandwidth of the LFM signal as the spectrogram in Fig. 12(a) shows. In the case of the TC-OLA-based LFM signal, CNJ is faced with a large spectrum spread that can reach up to $\frac{M}{R}f_1$ and therefore has to spread its power over a larger bandwidth compared to that of the LFM signal.

The response of the LFM-PC radar to CNJ at different values of Jamming to Signal Ratio (JSR) is shown in Fig. 13. At JSR = 25 dB, the jammer reduces the P_D of the LFM-PC radar to 50%. Increasing JSR to 35 dB can totally jam the LFM-PC radar.

In the jamming context, the TC-OLA-based LFM-PC radar has two main advantages: the overlapping segments that

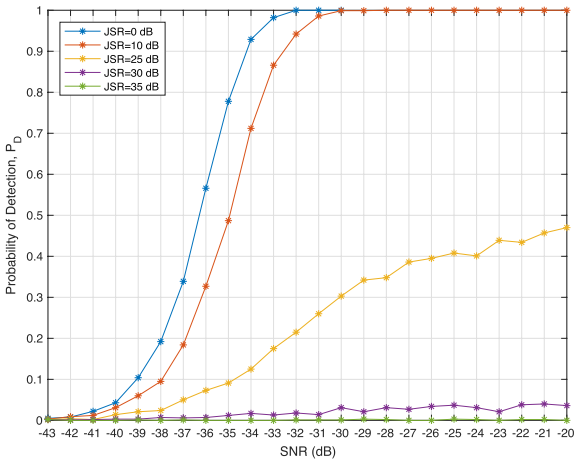

FIGURE 13. P_D vs *SNR* curve for traditional LFM-PC radar and under CNJ at *JSR* = 10, 25, 30, 35 dB.

increase the SNR by a factor of $\frac{M}{R}$, and the high sampling rate, which spreads the radar signal spectrum over a larger band that can reach $\frac{M}{R}f_1$. These two features are effective in reducing the impact of jamming on the new model. Fig. 14 and Fig. 15 display the effect of jamming on the performance of the TC-OLA-based LFM-PC at different $\frac{M}{R}$ values. We also plot the traditional LFM-PC in the same figures to ease the comparison and show the superiority of the proposed model.

Fig. 14 shows the performance of the proposed model at $\frac{M}{R} = 5$. The curves at JSR = 10 dB, 25 dB, and 30 dB are all very close to the curve without jamming (JSR = 0) and their probabilities of detection reach 100% at SNR ≈ -38 dB while the P_D decreases to $\approx$ 90% at JSR = 35 dB. Comparing these curves with those of the traditional LFM-PC radar, we have significant improvements in all JSR cases.

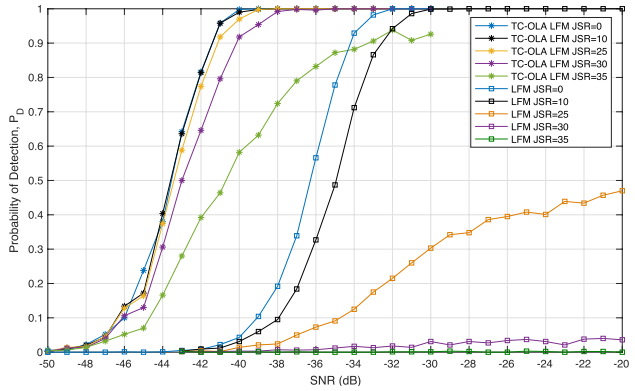

FIGURE 14. P_D vs *SNR* curve for LFM-PC and TC-OLA-based LFM-PC $\frac{M}{R} = 5$ under CNJ at $JSR = 10, 25, 30, 35$ dB.

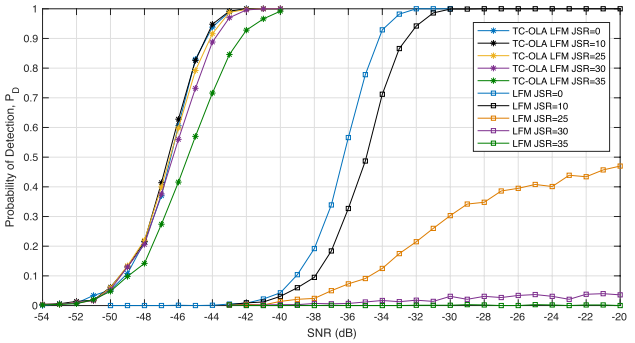

FIGURE 15. P_D vs *SNR* curve for LFM-PC and TC-OLA-based LFM-PC $\frac{M}{R} = 10$ under CNJ at $JSR = 10, 25, 30, 35$ dB.

If we increase $\frac{M}{R}$ to 10, all the probability of detection curves become all close to the one without jamming and saturate at -40 dB as shown in Fig. 15. The obvious solution for jamming our model is to raise the power level of the jamming signal by a factor proportional to $\frac{M}{R}$. Doing so, however, requires impractical high powers, especially for large values of $\frac{M}{R}$.

From a radar design perspective, the TC-OLA-based LFM model has the following features and advantages compared to the existing LFM radars:

1) Increase in the radar processing gain.
2) Ability to control gain increase by varying M and R.
3) Spread of the spectrum of the transmitted signal.
4) Ability to control the spectrum spread according to M and R.
5) Improve immunity against CNJ technique.
6) No need to change the radar signal processing blocks, namely MF, MTD, and CFAR,
7) The TC chirp signal produced is a scrambled version of the LFM chirp signal. This is an important feature as we transmit a kind of coded LFM signal without using any kind of coded sequence. For jammers that rely on the nature of LFM signal, they will not be able to extract our ''scrambled'' TC-OLA signal. whereas the radar processing block in other techniques must change according to new LFM signal parameters.
8) Preservation of the radar information, especially target range and Doppler, after descrambling the signal.
9) All the operations are done at lower sampling rate before TC processor and after OLA processor thus reducing processing costs and/or enabling the use of more complex algorithms.

If an LFM radar designer wants to achieve the same processing gain as our proposed model, the designer needs to increase the bandwidth to $\frac{M}{R}B$, which entails changing all the blocks involved in the LFM radar system to accommodate the new high rate, which misses out on most of the features and advantages mentioned above. More discussion is devoted to this in the next section.

VI. TC-OLA-BASED LFM RADAR VERSUS WIDEBAND LFM RADAR

The spreading of the signal in the case of TC-OLA does not contribute to either the processing gain or the resolution as the TC signal is transformed back to its original bandwidth after OLA. Therefore, comparing other LFM radar systems to TC-OLA based on the bandwidth is not fair. The figure of merit should be the processing gain and not the bandwidth. As we mentioned in the previous section, to achieve the same processing gain as TC-OLA-based LFM model, the designer needs to increase the bandwidth to $\frac{M}{R}B$. Although such a wideband LFM radar will miss out on most of the features we outlined in Section V, it is worth evaluating our proposed model against a wideband LFM radar with the bandwidth $\frac{M}{R}B$ (the bandwidth leading to the same processing gain as our proposed model) based on their noise and jamming performance, design implications and software defined radar implementations. In what follows, we will rely on Table 1 and 2 to support our discussion.

A. NOISE AND JAMMING PERFORMANCE

Assuming that the processing gain of a traditional LFM radar is G, the add-on TC-OLA technique into LFM radar increases the amplitude of the signal by amount of $\frac{M}{R}$, which means that the processing gain increases to $(\frac{M}{R})^2 G$. However, because of the $\frac{M}{R}$ increase of the AWGN variance, as a result of OLA processing, the total processing gain will be $(\frac{M}{R})G$ instead. In a wideband LFM radar, increasing the LFM radar bandwidth by a factor of $\frac{M}{R}$ leads to an increase in the amplitude of the signal by the amount of $\sqrt{\frac{M}{R}}$. This, in turn, increases the gain to be $(\frac{M}{R})G$. It should be emphasized that the extra processing gain of the proposed radar is from the overlapping segments while that of the wideband LFM is from expanding its bandwidth. As a result, both models have the same processing gain under AWGN as shown in Fig. 16.

In the case of CNJ, comparing the spectrogram of the TC-OLA model (see Fig. 6) with that of the wideband LFM-PC radar, shown in Fig. 17, we can see that the wideband LFM-PC radar covers all the frequencies in the bandwidth of interest, while our TC-OLA LFM model spreads the spectrum over a bandwidth equal to $\frac{M}{R}.f_1$ and not $\frac{M}{R}.B$ without covering

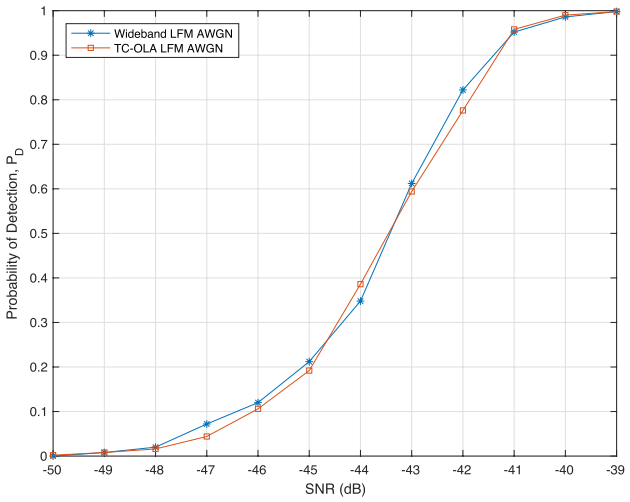

FIGURE 16. P_D vs *SNR* curve for wideband LFM-PC and TC-OLA-based LFM-PC, $\frac{M}{R} = 5$, under AWGN.

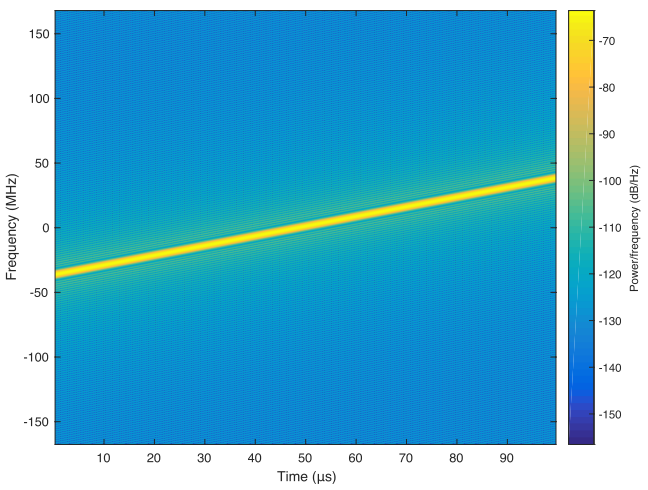

FIGURE 17. Spectrogram of the wideband LFM chirp signal with $B = 75$ MHz.

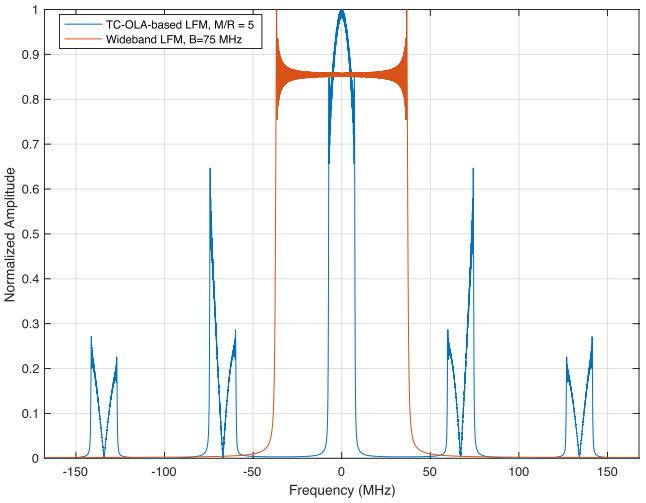

FIGURE 18. Spectrum of the wideband LFM chirp signal with $B = 75$ MHz and TC LFM signal, $\frac{M}{R} = 5$.

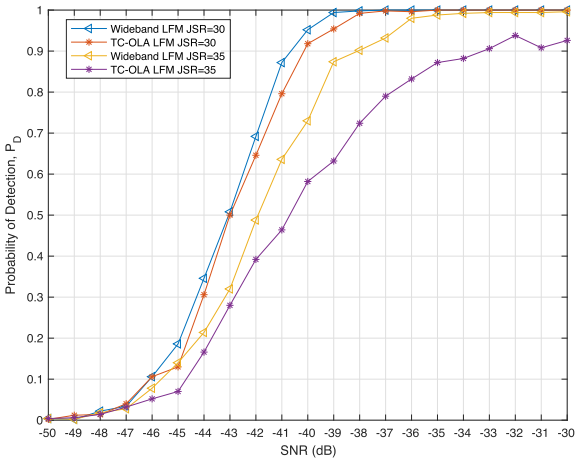

FIGURE 19. P_D vs *SNR* curve for wideband LFM-PC and TC-OLA-based LFM-PC $\frac{M}{R} = 5$ under CNJ at JSR = 30 dB.

all of its frequencies. To illustrate this further, we present the spectrum of both transmitted signals in Fig. 18. Therefore, in the TC-OLA case, the jammer has to choose between using extra power or reducing his power spectral density in order to cover all the band of the TC signal. Jamming the entire bandwidth of the TC-OLA signal can require f_1/B larger power than the wideband LFM signal.

Fig. 19 shows the performance of the two radars under high JSR, 30 dB and 35 dB. Although the MF bandwidth of the wideband LFM is $\frac{M}{R}$ larger than the TC-OLA MF bandwidth, the TC-OLA-based LFM radar has almost the same performance as the wideband LFM radar. The reason for the slight difference is attributed to the variance increase of the signal-correlated noise that the jammer introduces to the OLA processor.

B. DESIGN IMPLICATIONS

The TC-OLA technique has the privilege of increasing the radar system performance without the burden of changing and redesigning the existing radar system. Furthermore, the proposed TC-OLA radar system is much more flexible as it allows the radar designer to control the processing gain and the spectrum spread without changing the existing radar components. In fact, if $\frac{M}{R} = 1$, we are in the case of the traditional LFM. In contrast, in order to get the same processing gain as the TC-OLA-based LFM radar, the radar designer needs to redesign the entire radar system, transmitter, and receiver. This, in turn, increases the complexity of the system as the entire system has to deal with high data rates.

It is worth mentioning, however, that the wideband LFM radar is better in the range resolution by the amount of the expanding factor $\frac{M}{R}$.

C. SOFTWARE DEFINED RADAR IMPLEMENTATION

Software defined radar (SDR) is an emerging field that permits the radar designers to implement most of the radar components using software [22], [23]. It is worth therefore comparing TC-OLA-based LFM and wideband LFM radars according to their SDR implementation. As far as we know, the only limitation of designing an SDR TC-OLA-based LFM is the maximum available SDR sampling rate. On the other hand, in addition to the sampling rate limitation, the SDR wideband LFM radar designer will face a challenge since the entire system is dealing with high data rates, especially for higher $\frac{M}{R}$ ratios. In fact, at the receiver, MF has a high rate LFM reference signal. If MF is implemented in time domain, it would be very challenging given the huge number of multiplications and additions involved. Moreover, in the MTD processor, since the digital received signal is stored in 2-D array, a designer has extra limitations that will require additional SDR resources. Therefore, TC-OLA offers an attractive way to implement LFM on SDR with minimal resources compared to wideband LFM.

VII. CONCLUSION AND FUTURE WORK

In this paper, we have introduced a new radar model that integrates the TC-OLA technique into the LFM-PC radar. The proposed TC-OLA-based LFM-PC radar allows the radar designer to control the SNR, as well as the spreading of the spectrum, by varying the two fundamental TC-OLA parameters: the segment length M and the hop size R. The traditional LFM-PC radar has been validated under specific parameters in order to compare it with the TC-OLA-based LFM-PC radar. The two models were investigated under AWGN as well as CNJ. TC-OLA-based LFM-PC is superior to LFM-PC for both AWGN and jamming while maintaining the same information as LFM-PC. For CNJ to be effective against the new radar model, the jammer has to increase its power significantly. Furthermore, the proposed radar model does not require changing the main radar components, namely MF, MTD, and CFAR as it relies on high sample rates only at TC and before OLA. Moreover, the spread of the spectrum introduced by the proposed model is partial as it does not extend to the rest of the radar components.

The comparison between the proposed model and wideband LFM radar, under the same processing gain, based on noise and jamming performance, design complexity and software-defined radar implementation is discussed. Although the wideband LFM has better resolution, its AWGN performance are the same as the proposed model, and its CNJ performance are only slightly better. In addition, the wideband LFM radar requires redesigning the entire radar system to accommodate the higher bandwidth (therefore higher sampling rates), and a challenging SDR implementation.

Research on improving the TC-OLA technique in LFM radar systems and testing it in different background conditions and multi-target situations are ongoing. The effect of segment of length and the hopping size on the spectrum spread is being investigated and quantified. Finally, the Software Defined Radar (SDR) implementation of our TC-OLA-based LFM is underway.

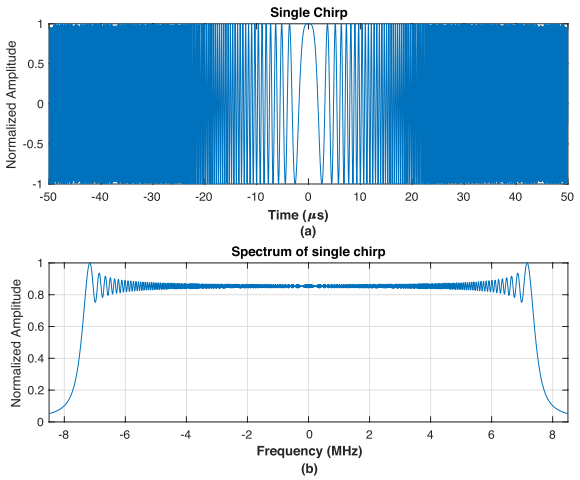

FIGURE 20. Radar LFM chirp signal: (a) Single pulse in time domain. (b) Single pulse in frequency domain.

APPENDIX

A. VERIFICATION OF LFM-PC RADAR MODEL

The LFM-PC radar model (Fig. 1) was verified using MATLAB simulations with the radar parameters specified from Table 1.

The LFM waveform is generated as depicted in Fig. 20 (a). Its spectrum is shown in Fig. 20 (b). The simulated LFM chirp signal has a duration of 100 μs, and a bandwidth of 15 MHz.

The output of the MF is given by:

$$y(t) = FFT^{-1}\{FFT\{s(t) \otimes h(t)\}\}, \tag{10}$$

where $s(t)$ is the input signal, and $h(t)$ is the MF impulse response, which is the stored replica of the LFM radar signal. The impulse response $h(t)$ is given by [2]:

$$h(t) = K \times s^*(t_0 - t), \tag{11}$$

where K is a constant, t_0 is a time delay and $s^*(t_0 - t)$ is the inverse delayed replica of the conjugate of the signal. For the filter to be causal, the delay t_0 must be greater than or equal to the duration of the signal $s(t)$ [24]. Therefore, the causality of the MF gives a minimum delay of 100 μs, corresponding to the pulse duration. According to the target range in Table 1, the time delay of the target is 238.4 μs. This gives a total delay of 338.4 μs as can be seen from the output of the simulated MF shown in Fig. 21 (a). In [2], [10], [25], and [26], the LFM MF output has a peak sidelobe between -13 and -13.5 dB. This agrees with our simulation as Fig. 21 (b) shows.

The output of MF is passed through MTD processor. MTD produces a 2-D array with rows corresponding to the Doppler cells and columns corresponding to the range cells as shown in Fig. 22. In Table 1, PRI is taken to be 0.5 ms (PRF is, therefore, equal to 2000 Hz), and the target Doppler frequency is equal to 7000 Hz. Therefore, we expect an ambiguous target

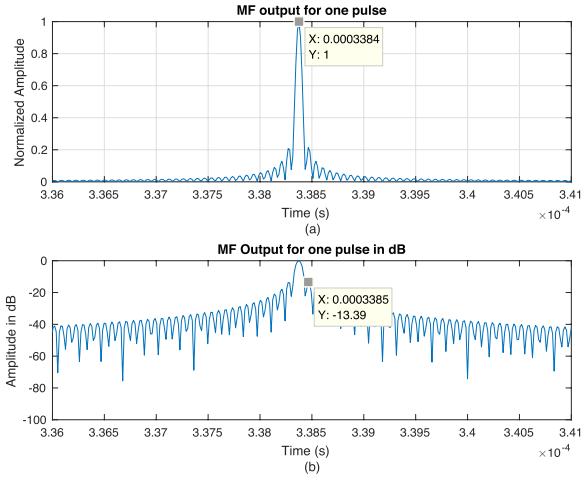

FIGURE 21. (a) The output of the MF with total delay. (b) The output of MF in dB indicating side lobe level.

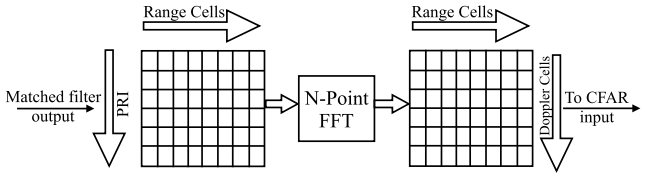

FIGURE 22. Storage of radar signal in different domains for moving target detector (MTD).

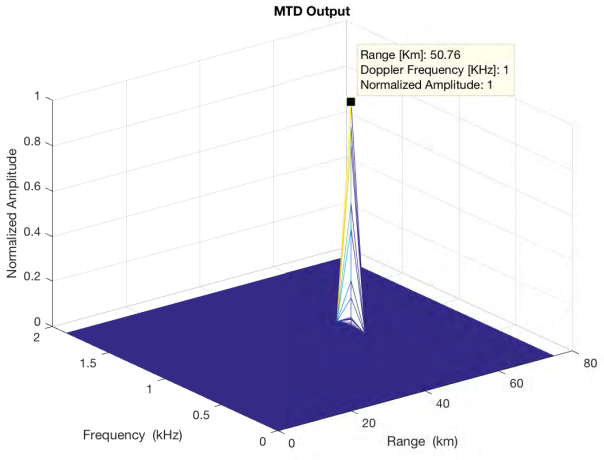

FIGURE 23. Output of MTD.

Doppler frequency of 1000 Hz. In Fig. 23, the target appears at the 9^{th} Doppler cell, which means the Doppler frequency is between 1000 Hz and 1125 Hz according to the model Doppler resolution at the 50.76 km range. These values are consistent with the ambiguous target Doppler frequency.

Based on the output of the MTD processor, CFAR computes the adaptive threshold at each Doppler cell to maintain a false alarm rate, P_{fa}, 10^{-6}, a typical value in radars [1], [3], [11]. The CFAR processor introduces an additional delay corresponding to the number of the window

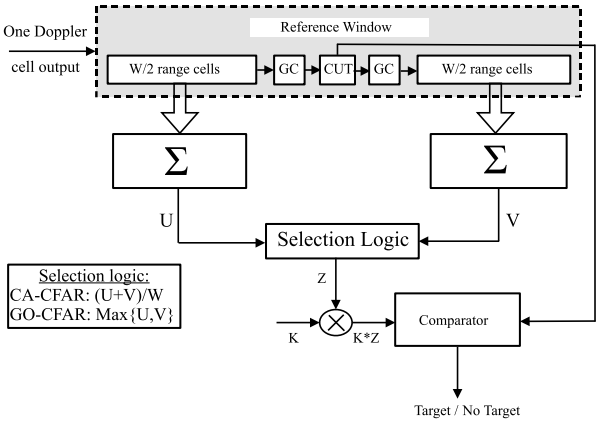

FIGURE 24. CA-CFAR and GO-CFAR Detectors.

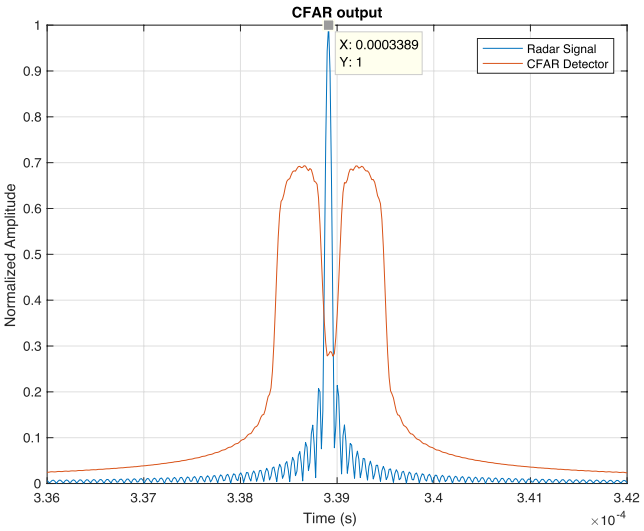

FIGURE 25. CA-CFAR detector.

cells preceding the CUT cell. This delay is equivalent to 0.53644 μs (80.4663 m in range) and is added to the previous delays to give a total delay of 338.95 μs, which can be compensated for in the radar display. Fig. 24 shows the two types of detectors used, namely CA-CFAR and GO-CFAR. Fig. 25 shows the CA-CFAR output as well as the total delay of the radar model.

Recalling the processing gain of each stage in the radar model (see Section II), we expect a compression gain increase of 31.7 dB of MF over the theoretical envelope detector and an extra gain of 12 dB coming from the 16 pulses passing through MTD. The overall processing gain should, therefore, be 43.7 dB.

The P_D vs SNR curve of LFM-PC radar model with CA-CFAR and GO-CFAR detectors is shown in Fig. 26. The detection of both CFAR processors is lower than the theoretical detection. The reason for that is the target-return side lobes appearing in the CFAR processor window and affecting the CFAR threshold. From Fig. 26, CA-CFAR is slightly better than GO-CFAR. Based on the structure of the two detectors,

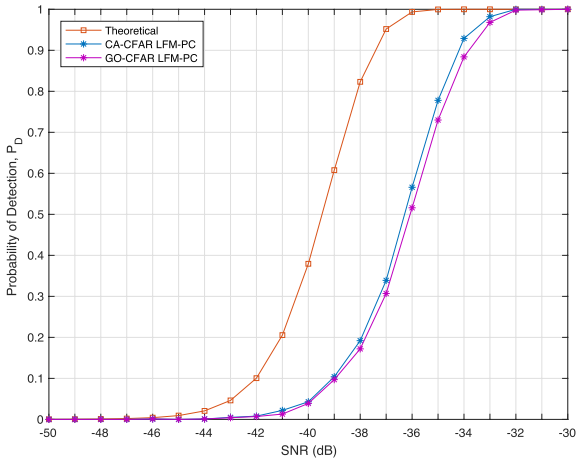

FIGURE 26. P_D vs *SNR* curve for Theoretical, CA-CFAR, and GO-CFAR of LFM-PC at $P_{fa} = 10^{-6}$ under AWGN.

the threshold level of the CA-CFAR is computed using an average operator while that of GO-CFAR is obtained using a maximum operator. As such, the CA-CFAR threshold is lower and leads therefore to higher detection for the same P_{fa}.

B. DOPPLER SHIFT UNDER TC-OLA

From Subsection III-A, we can deduce the following facts:

- The number of repeated samples equal to $\frac{M}{R}$.
- The samples are repeated each $M - R$ samples.
- The number of segments that contain repeated segments equal to $\frac{M}{R} - 1$.

Let $f(n)$ be the sampled version of the Doppler shift, f_d, multiplied with the radar received signal:

$$f(n) = e^{j2\pi f_d n/f_2}, \tag{12}$$

where:

- $f_d = \frac{2v_r}{\lambda}$, v_r is the target radial velocity and $\lambda = \frac{c}{f_c}$, c is speed of light and f_c is the radar carrier frequency.
- $f_2 = \frac{M}{R} f_1$ is the higher sampling rate, f_1 is the sampling rate of the traditional LFM radar.

The OLA processor adds consecutive segments of length M that is shifted to the right by R with respect to its preceding segment. The distance between the index of the sample $f(n)$ and the index of its farthest repeated sample is $(M - R)(\frac{M}{R} - 1)$. Therefore, the ratio between $f(n)$ and its repeated sample Doppler shift is:

$$\frac{f(n + (M-R)(\frac{M}{R} - 1))}{f(n)} = \frac{e^{\frac{j2\pi(n+(M-R)(\frac{M}{R}-1))}{f_2} f_d}}{e^{\frac{j2\pi n}{f_2} f_d}} = e^{\frac{j2\pi(M-R)(\frac{M}{R}-1)}{f_2} f_d}.$$

For the ratio to be close to 1, we need the following to be true:

$$\frac{(M-R)(\frac{M}{R} - 1)}{f_2} f_d \ll 1, \tag{13}$$

which is equivalent to

$$f_d \ll \frac{f_2}{(M-R)(\frac{M}{R} - 1)} \tag{14}$$

Substitute f_2 by its expression, we get:

$$f_d \ll \frac{\frac{M}{R} f_1}{(M-R)(\frac{M}{R} - 1)}$$
$$f_d \ll \frac{M f_1}{(M-R)^2}$$
$$\frac{M}{(M-R)^2} \gg \frac{f_d}{f_1} \tag{15}$$

From Eq. 15, the worst case happens if $M \gg R$. In this case, we have

$$\frac{1}{M} \gg \frac{f_d}{f_1}$$
$$M \ll \frac{f_d}{f_1}, \tag{16}$$

Finally, We can write the final equation as:

$$M \ll \frac{f_1}{f_c} \frac{c}{2v_r} \tag{17}$$

ACKNOWLEDGMENTS

The authors would like to thank WestGrid and Compute Canada for their valuable computational resources and support. They would also like to thank Dr. S. Harrison, A. Abouelfadl, and Dr. S. G. Tanyer for their valuable discussions and inputs. The reviewers comments were essential in improving the quality of the paper by clarifying many points, and adding Section VI and Subsection VII-B in the appendix.

REFERENCES

[1] M. I. Skolnik, *Introduction to Radar Systems*. New York, NY, USA: McGraw Hill, 2001.
[2] B. R. Mahafza, *Radar Signal Analysis and Processing Using MATLAB*. Boca Raton, FL, USA: CRC Press, 2016.
[3] M. I. Skolnik, *Radar Handbook*, 3rd ed. New York, NY, USA: McGraw-Hill, 2008.
[4] S. Harrison and P. F. Driessen, "Novel UWB and spread spectrum system using time compression and overlap-add techniques," *IEEE Access*, vol. 2, pp. 1092–1105, 2014.
[5] S. T. Harrison and P. F. Driessen, "Time-compression overlap add: Description and implementation," in *Proc. IEEE Pacific Rim Conf. Commun., Comput. Signal Process. (PACRIM)*, Aug. 2015, pp. 64–69.
[6] W. Ye, H. Ruan, S. Zhang, and L. Yan, "Study of noise jamming based on convolution modulation to SAR," in *Proc. Int. Conf. Comput., Mechatronics, Control Electron. Eng.*, vol. 6, Aug. 2010, pp. 169–172.
[7] J. Jiang, Y. Wu, and H. Wang, "Analysis of active noise jamming against synthetic aperture radar ground moving target indication," in *Proc. 8th Int. Congr. Image Signal Process. (CISP)*, Oct. 2015, pp. 1530–1535.
[8] B. Lv, "Simulation study of noise convolution jamming countering to sar," in *Proc. Int. Conf. Comput. Design Appl. (ICCDA)*, vol. 4, Jun. 2010, pp. V4–130.
[9] M. A. Richards, J. A. Scheer, and W. A. Holm, *Principles of Modern Radar*. Raleigh, NC, USA: SciTech, 2010.
[10] M. A. Richards, *Fundamentals of Radar Signal Processing*. New York, NY, USA: McGraw-Hill, Jun. 2005.
[11] G. Galati, *Advanced Radar Techniques and Systems*. Stevenage, U.K.: Peregrinus, 1993.
[12] N. Friedman and United States Naval Institute, *The Naval Institute Guide to World Naval Weapons Systems*. Annapolis, MD, USA: Naval Institute Press, 1989.

[13] G. Galati, *100 Years of Radar*. Cham, Switzerland: Springer, 2015.
[14] A. Abouelfadl, A. M. Samir, M. Fathy, and A. H. Asseesy, "Performance analysis of LFM pulse compression radar under effect of convolution noise jamming," in *Proc. 33rd Nat. Radio Sci. Conf. (NRSC)*, Feb. 2016, pp. 282–289.
[15] D. C. Schleher, *Electronic Warfare in the Information Age*. Norwood, MA, USA: Artech House, Jan. 1999.
[16] L. Tan and J. Jiang, *Digital Signal Processing: Fundamentals and Applications*, 2nd ed. Boston, MA, USA: Academic, 2013.
[17] Migflug.com. *The 10 Fastest Aircraft in the World, From Su-27 Flanker to X-15*. Accessed: Jun. 23, 2017. [Online]. Available: http://www.migflug.com/jetflights/the-10-fastest-aircraft-in-the-w%orld.html
[18] C. Erdmann *et al.*, "A 330 mW 14 b 6.8 GS/s dualmode RF DAC in 16 nm FinFET achieving −70.8 dBc ACPR in a 20 MHz channel at 5.2 GHz," *IEEE Int. Solid-State Circuits Conf. (ISSCC) Dig. Tech. Papers*, Feb. 2017, pp. 280–281.
[19] B. Vaz *et al.*, "A 13 b 4 GS/s digitally assisted dynamic 3-stage asynchronous pipelined-SAR ADC," in *IEEE Int. Solid-State Circuits Conf. (ISSCC) Dig. Tech. Papers*, Feb. 2017, pp. 276–277.
[20] Z. Yu and Y. Shao-quan, "Convolution jamming technique countering LFM radar," *J. Electron. Inf. Technol.*, vol. 6, p. 030, Jun. 2007.
[21] H. Hu and N. Wei, "A study of GPS jamming and anti-jamming," in *Proc. 2nd Int. Conf. Power Electron. Intell. Transp. Syst. (PEITS)*, vol. 1. Dec. 2009, pp. 388–391.
[22] J. Hershberger, T. Pratt, and R. Kossler, "Implementations of coherent software-defined dual-polarized radars," *IEEE Trans. Microw. Theory Techn.*, vol. 65, no. 5, pp. 1673–1681, May 2017.
[23] B. Tuysuz, J. Urbina, and F. D. Lind, "Development of a passive VHF radar system using software-defined radio for equatorial plasma instability studies," *Radio Sci.*, vol. 48, no. 4, pp. 416–426, 2013.
[24] N. Levanon and E. Mozeson, *Radar Signals*. Hoboken, NJ, USA: Wiley, 2004.
[25] H. O. Ramp and E. R. Wingrove, "Principles of pulse compression," *IRE Trans. Military Electron.*, vol. 1051, no. 2, pp. 109–116, Apr. 1961.
[26] R. Milleit, "A matched-filter pulse-compression system using a nonlinear FM waveform," *IEEE Trans. Aerosp. Electron. Syst.*, vol. AES-6, no. 1, pp. 73–78, Jan. 1970.

AHMED YOUSSEF received the M.A.Sc. degree from the Military Technical College, Egypt, in 2012. He is currently pursuing the Ph.D. degree in electrical and computer engineering with the University of Victoria, Victoria, BC, Canada. He was a Teacher Assistant for four years with the Radar Department, Military Technical College. His research interests include digital signal processing, radar signal processing, and digital communications.

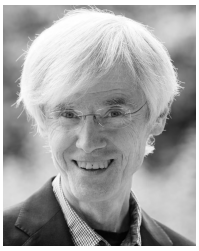

PETER F. DRIESSEN received the Ph.D. degree from The University of British Columbia, Vancouver, BC, Canada. He was with various companies in Vancouver for five years, designing modems for data communications. He joined the University of Victoria, Victoria, BC, Canada, where he is currently a Professor of electrical and computer engineering, with cross appointments in music and computer science. He was with the *AT&T* Bell Laboratories, Murray Hill, NJ, USA, where he was involved in wireless communications systems. He is currently a Professor of electrical and computer engineering with the University of Victoria. He was the Papers Co-Chair of the International Computer Music Conference held in Cuba. He served on the Board of Governors of the University of Victoria for six years.

FAYEZ GEBALI received the B.Sc. degree (Hons.) in electrical engineering from Cairo University, the B.Sc. degree (Hons.) in mathematics from Ain Shams University, and the Ph.D. degree in electrical engineering from The University of British Columbia, where he was a holder of an NSERC Postgraduate Scholarship. He is currently a Professor of electrical and computer engineering with the University of Victoria. His research interests include parallel algorithms, systems-on-chip, digital communications, and computer arithmetic and signal processing for RADAR systems.

BELAID MOA received the B.Sc. degree in electrical engineering from École Hassania des Travaux Publics, Casablanca, Morocco, the M.Eng. degree in electronics and signal processing from École Nationale Supérieure d'électronique, d'électrotechnique, d'informatique, d'hydraulique et des Télécommunications, Toulouse, France, the DEA Diploma degree in networks and networks from the Institute National Polytechnique de Toulouse, Toulouse, and the Ph.D. degree in computer science from the University of Victoria, Victoria, BC, Canada. He is currently a Research Computing Specialist with the Compute Canada/WestGrid/University Systems, University of Victoria. He has authored or co-authored many research articles and conference proceedings in various journals.